Solar Energy 196 (2020) 336–345

Contents lists available at ScienceDirect

Solar Energy

journal homepage: www.elsevier.com/locate/solener

A copula-based Bayesian method for probabilistic solar power forecasting

Hossein Panamtash[a], Qun Zhou[a,*], Tao Hong[b], Zhihua Qu[a], Kristopher O. Davis[c]

[a] Department of Electrical Engineering, University of Central Florida, Orlando, FL 32816, USA
[b] Department of System Engineering and Engineering Management, University of North Carolina at Charlotte, Charlotte, NC 28223, USA
[c] Department of Material Science and Engineering, University of Central Florida, Orlando, FL 32816, USA

ARTICLE INFO

Keywords:
Bayesian inference
Solar power forecasting
Copulas
Probabilistic forecasting

ABSTRACT

With increased penetration of solar energy sources, solar power forecasting has become more crucial and challenging. This paper proposes a copula-based Bayesian approach to improve probabilistic solar power forecasting by capturing the joint distribution between solar power and ambient temperature. A prior forecast distribution is first obtained using different underlying point forecasting models. Parametric and empirical copulas of solar power and temperature are then developed to update the prior distribution to the posterior forecast distribution. A public solar power database is used to demonstrate effectiveness of the proposed method. Numerical results show that the copula-based Bayesian method outperforms the forecasting method that directly uses temperature as a feature. The Bayesian method is also compared with persistent models and show improved performance. This article includes supplementary material (data and code) for reproducibility.

1. Introduction

The penetration of solar power is rapidly growing over the last few years (Marcy, 2019). Due to the intermittency of solar sources, there is a pressing need for solar power forecasting. The quality of forecasts provided to system operators has a significant impact on the power grid security as well as the operational and planning cost (Murata et al., 2018). Furthermore, an accurate and detailed representation of forecasting uncertainties is critical for system operators to determine the trade-off between risk and return, leading to a better decision-making process in the renewable-penetrated power grid (Hong et al., 2019).

Solar power forecasting is unique in the energy forecasting domain in terms of exogenous data usage, such as sky images and Numerical Weather Prediction (NWP). For example, Pedro et al. use sky images to improve solar irradiance forecast (Pedro et al., 2018), and a detection method for clear sky images is developed considering aerosol effects in (Pawar et al., 2019). NWPs are used in a forecasting model combined with multivariate statistical learning to forecast solar irradiance (Verbois et al., 2018). Additionally, NWP are used in Kernel conditional density estimation for global horizontal irradiance (GHI) forecasts to correct model-led errors (Yang, 2019b).

These exogenous data are also employed in generation of spatio-temporal forecasts. For example, atmospheric data such as cloud coverage and height, wind speed and atmospheric pressure are used to forecast irradiance over spatial dimensions (Bright et al., 2017). In recent years many efforts have been dedicated to spatio-temporal models that generate forecasts for several nearby locations. For example (Yang et al., 2017) use an NWP-based day-ahead forecast reconciliation method to generate more accurate forecasts that aggregate consistently with higher level forecasts. An improved probabilistic model is proposed to study how solar irradiance is correlated and aggregated over a network (Widén et al., 2017). André et al. (2019) use a spatio-temporal vector autoregressive model combined with a statistical process for short-term forecasting of GHI.

In contrast to the common practice of using exogenous data as inputs to the forecast model, we propose a Bayesian forecasting approach where exogenous inputs are treated as random variables. We selected ambient temperature as the exogenous input, but the proposed method can be generalized to include other available inputs. As the first step, historical solar power data are used to generate probabilistic forecasts. Probabilistic forecasting is gaining attention in the energy sector (Fliess et al., 2018; Saint-Drenan et al., 2017) in recent years. Commonly used models for probabilistic forecasting are Gaussian process and quantile regression (Shepero et al., 2018; van der Meer et al., 2018). A Markov-chain mixture model is employed in (Munkhammar et al., 2019) for clear sky GHI forecasting. Also, (Pedro et al., 2018) generates probabilistic forecast quantiles using persistant ensemble, K-nearest neighbors and gradient boosting (GB). Furthermore, probabilistic forecasting can offer more information to assist power system operators make decisions based on different possible scenarios. For example, balancing

* Corresponding author.
E-mail address: qun.zhou@ucf.com (Q. Zhou).

https://doi.org/10.1016/j.solener.2019.11.079
Received 16 September 2019; Received in revised form 22 November 2019; Accepted 23 November 2019
Available online 20 December 2019
0038-092X/

between load and generation in power systems is crucial for maintaining the frequency. Power system operations considering the uncertainties associated with loads and renewable generation is very challenging (Hong et al., 2019). Power system operators can greatly benefit from probabilistic forecasting of load, renewable generation and net load to plan for generation scheduling.

After the prior probabilistic forecasts are obtained, we apply the Bayesian rule to improve forecasts and obtain posterior probabilistic forecasts. The proposed Bayesian forecasting uses copulas to obtain the joint probability distribution of solar power and temperature. Copula theory is popular in high-dimensional statistical analysis as it allows to separately model variable dependencies and marginal distributions. Sklar's theorem states that any multivariate joint distribution can be written by multiple univariate marginal distributions and a copula that describes the dependency structure among those variables (Nelsen, 2006). Copula is a powerful tool in finance (Koopman et al., 2018) and recently has been applied for energy forecasting (Munkhammar et al., 2017; Panamtash and Zhou, 2018). Empirical copulas are constructed to estimate the joint distribution between wind power and wind speed (Bessa et al., 2012). Munkhammar et al. also use empirical copulas to model the dependence of clear sky index at different locations (Munkhammar et al., 2017). Our prior work used empirical copulas to achieve coherent hierarchical forecasts for different systems levels, i.e., bus level, community level, and substation level (Panamtash and Zhou, 2018).

Note that our paper is focused on single-location probabilistic forecasting which is much needed when considering grid-connected PV-battery storage systems and home energy management system for bundled PV-battery systems in residential homes (Hemmati and Saboori, 2017; Zheng et al., 2018). Accurate forecasting of PV would benefit battery scheduling and reduce energy dispatch cost.

The remainder of this paper is organized as follows. Section 2 reviews the Bayesian forecasting framework. Section 3 describes the dataset and the procedure of producing prior probabilistic forecast distribution using five different forecasting models. Section 4 constructs parametric and empirical copulas for solar power and ambient temperature, and applies them to derive the posterior forecast distribution. Section 5 discusses the probabilistic forecast evaluation. Section 6 presents numerical results. Section 7 provides concluding remarks and future work.

2. Bayesian forecasting

The copulas-based Bayesian forecasting model aims to capture the joint probability distribution of exogenous data and solar power.

Fig. 1 illustrates the differences between the Bayesian method and the forecasting method that uses temperature as a feature (TaaF). In TaaF forecasting, the temperature data are directly fed to the forecasting model to compute forecasts for solar power. In contrast, the purpose of Bayesian forecasting is to derive posterior distribution based on conditional probability density of power given temperature. Conditional probability density function (PDF) of a random variable X, given another random variable Y, is written by:

$$f\left(x\middle|Y=y\right)=\frac{f_{XY}(x,y)}{f_Y(y)}, \tag{1}$$

where $f_{XY}(x,y)$ is the joint probability distribution of X and Y and $f_Y(y)$ is the marginal distribution function of Y.

This paper aims to test the hypothesis that Bayesian forecasting outperforms the solar power forecasting method that uses exogenous data as input features. For a comprehensive assessment, this paper applies five commonly used point forecasting models and extends the results to probabilistic forecasts, which form the prior forecast distribution for solar power. To derive the posterior forecast distribution, the joint probability distribution between temperature and solar power

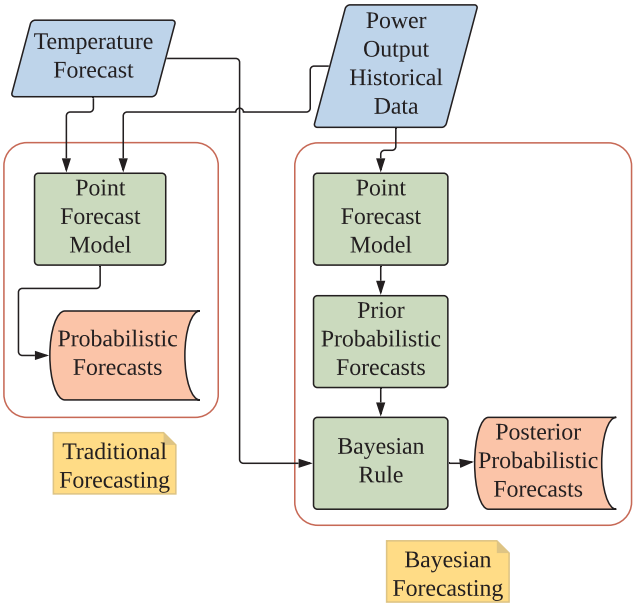

Fig. 1. Bayesian forecasting vs TaaF forecasting.

is developed using two-dimensional parametric and empirical copulas. Fig. 2 illustrates the procedure of deriving different types of copulas, i.e., Gaussian, t, Frank, and empirical copulas, and updating the probabilistic forecasts generated from five different models, i.e., artificial neural network (ANN), GB, multiple linear regression (MLR), random forest (RF), and autoregressive integrated moving average (ARIMA).

3. Prior probabilistic forecasts

This section describes the solar power dataset used in the paper and how to generate probabilistic forecasts of solar power based on historical data. Five models are used separately to produce point forecasts. Then for each model, point forecasts are extended to probabilistic forecasts. As a result, the prior probabilistic forecast in Bayesian forecasting is obtained.

3.1. Dataset

3.1.1. Solar power dataset

The solar power output data are downloaded from the Florida Solar Energy Center (FSEC) database (Ino, Lynn et al., 2006, Davis et al., 2013). The FSEC database is an online public database with 106 PV sites installed at locations throughout the state of Florida. Each PV site on the FSEC database contains various types of data such as power output, temperature, irradiance, and wind speed. We noted that some data are missing, and hence selected the following four PV sites with relatively less missing data:

- The Bayshore elementary school is located at 1661 SW Bayshore Blvd, Port St. Lucie, FL 34984, USA.
- The Crawfordville elementary school is located at 379 Arran Rd, Crawfordville, FL 32327, USA.
- The Deerlake middle school is located at 9902 Deer Lake W, Tallahassee, FL 32312, USA.
- The Dunnellon high school is located at 10055 SW 180th Avenue Rd, Dunnellon, FL 34432, USA.

All of the PV sites have a capacity of 10 KW. The data are recorded in 15-min intervals. Solar power output and weather data in the years 2015 and 2016 are used in this study. The scatter plot of 2015 data is shown in Fig. 3. It is observed that the correlation does exist between

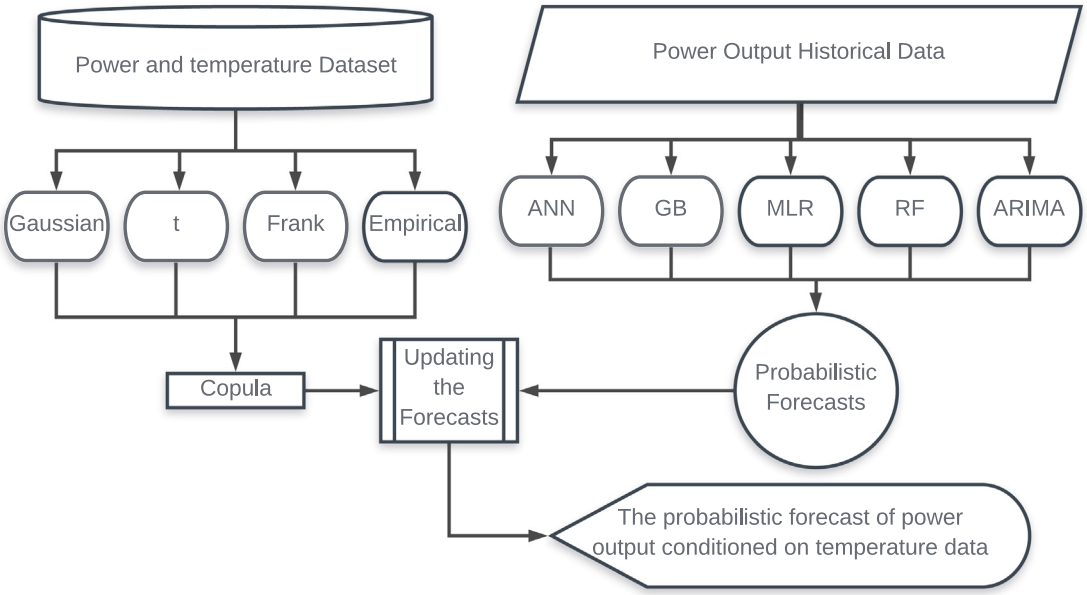

Fig. 2. Copula-based Bayesian solar power forecasting.

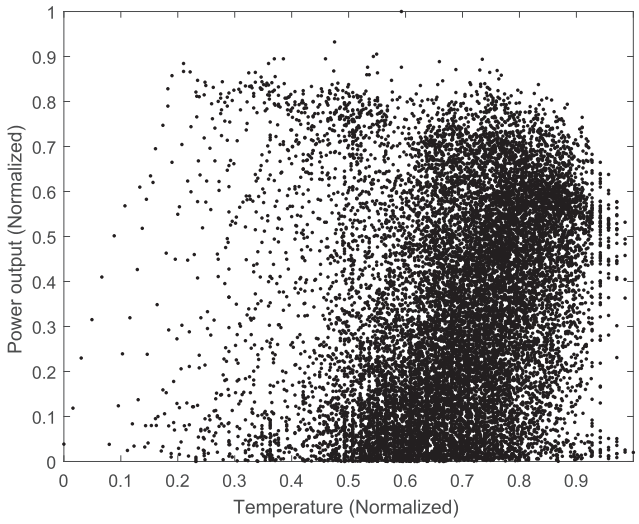

Fig. 3. Scatter plot of power output and temperature from 2016 at Bayshore elementary school.

solar power and temperature, but is nonlinear and not as strong. This indicates that a simple treatment of temperature as a feature in the forecasting may not render a good performance. Hence, a Bayesian method is used to handle the complication and later verified in the paper.

3.1.2. Dataset quality control

The quality of the solar power dataset used for this study has been checked against criteria based on a statistical clear sky (CS) model (Engerer and Mills, 2014). The clear sky model uses the 30 days of data preceding the test day and selects the 95th percentile from the measurements for different times of the day to shape the CS curve.

- Maximum k_{pv}

  The clear sky index as defined in (Engerer and Mills, 2014):

$$K_{PV} = \frac{P_M}{P_{CS}}, \tag{2}$$

  where P_M is the measured power and P_{CS} is the clear sky model power. If the power output exceeds 1.05 times the CS model the data point is flagged.

- Daily Average Ratio of Power

  The ratio of average measured power to the average CS power is calculated for each day. A small ratio may indicate extreme overcast or detect measurement system failure or covering of the PV panels by dust or snow.

$$R_{DAP} = \frac{\sum_{t=00:00}^{23:45} P_M}{\sum_{t=00:00}^{23:45} P_{CS}}, \tag{3}$$

  In this work, the days with data points with $R_{DAP} < 0.1$ are flagged.

- Variance limit

  Eq. 4 imposes variance limits. If the variance of power normalized by the extraterrestrial irradiance exceeds the chosen limits the day is flagged. The variance interval is defined as below (Killinger et al., 2017):

$$\frac{1}{8}\mu\left(\frac{P_M}{E_{ext}}\right) \leqslant \sigma\left(\frac{P_M}{E_{ext}}\right) \leq 0.3, \tag{4}$$

  where μ and σ represent the mean and standard deviation for one day of data and E_{ext} is the extraterrestrial irradiance normalized by 1 kW/m^2.

The three criteria are used to check the quality of the data. Table 1 shows how much of the data used in this study are flagged according to each criteria in all the locations studied in this work.

Table 1
Percentage of total data flagged by each quality control criteria.

Location	Maximum k_PV	Daily average	Variance limit
1	2.38%	0.28%	0%
2	4.62%	2.09%	0.29%
3	3.44%	7.16%	0%
4	4.53%	1.19%	0.3%

3.2. Point forecasting

Five forecasting models are used to generate point forecasts, i.e., ANN, GB, MLR, RF, and ARIMA. The inputs are the past instances and the outputs are one-step forecasts of solar power.

- *Multiple Linear Regression.* MLR models the relation between output variable y and a set of d-dimensional input vector $x_1, x_2, ...,x_d$ by fitting a linear equation on n data points:

$$y_i = \beta_0 + \beta_1 x_{i,1} + \beta_2 x_{i,2} + ...+\beta_d x_{i,d} + \epsilon_i, \quad i = 1, ...,n, \tag{5}$$

  where $\beta_0, \beta_1, ...,\beta_d$ are the regression coefficients and ϵ_i is the error term. The coefficients can be estimated by minimizing the total errors using the ordinary least squares method.
- *Artificial Neural Networks.* ANN is a machine learning model inspired by the human nervous system. These networks are universal function approximators that map the relationship between the input and output using multiple neurons. The weights of these neurons are updated using back-propagation. In this study, different configurations of neural networks are experimented. The number of layers and neurons are optimally selected for each case based on the training set.
- *Gradient Boosting.* The objective of gradient boosting is to minimize the loss of the model by adding weak learners using a gradient descent procedure. GB algorithms construct stage-wise additive models with one new weak learner added at a time. Weak learners can take various formats. One commonly used weak learner is the decision trees. For example, regression trees are used to output real values that can be added together. Subsequent models are added to fit the residuals in the forecasts. GB can be formulated as:

$$F_{m+1}(x) = F_m(x) + h(x) = y. \tag{6}$$

  where F_m is the model for the m^{th} iteration and $h(x)$ is the weak learner added to improve the model. In each iteration the weak learner $h(\cdot)$ is fitted to the error term $y - F_m(x)$ which is the gradient of the square error loss function $\frac{1}{2}(y - F_m(x))^2$.
- *Random Forests.* Random forests is an ensemble method used to generate forecast models for both classification and regression problems. Random forests use multiple learning models to create uncorrelated decision trees. Given a set of training data $X = [x_1, ...,x_n]$ with outputs $Y = [y_1, ...,y_n]$, B subset groups of data (X_b, Y_b) are randomly chosen and a decision tree is fitted to each one using a randomly selected set of features (f_b). In order to forecast the output for a new set of data x', the forecasts from all the fitted trees are averaged:

$$f(x') = \frac{1}{B}\sum_{b=1}^{B} f_b(x'). \tag{7}$$

  The random selection of the data and feature is done to prevent any correlation between the trees. Averaging the results of a number of trees resolve the issue of overfitting associated with decision trees.
- *Autoregressive Integrated Moving Average.* The autoregressive model is a time series model that uses the past instances of data to forecast future outcomes. The moving average (MA) model forecasts the next step by a weighted average of past instances of a stochastic variable. The ARIMA model, a combination of AR, MA, and a differencing step, can be expressed as:

$$\hat{y}_t - y_{t-1} = \sum_{i=1}^{n} p_i y_{t-i} + \sum_{j=1}^{m} q_j e_{t-j}, \tag{8}$$

  where $\hat{y}_t$ is the prediction of output for the time t, y_{t-i} are the lagged instances of the output, p_i are the coefficients associated with the previous outputs, e_{t-j} are white noise error terms for each time and q_j are the coefficients for each past error.

3.3. Extend to probabilistic forecasts

The values obtained from each point forecasting model need to be extended to probabilistic forecasts. This paper compares two different methods for probabilistic forecasting and selects the most accurate to create the probabilistic forecasts.

3.3.1. Gaussian distribution

Probabilistic forecasts can be obtained by assuming Gaussian distribution around the mean of point forecasts:

$$f\left(p \middle| \mu, \sigma^2\right) = \frac{1}{\sqrt{2\pi\sigma^2}} e^{-\frac{(p-\mu)^2}{2\sigma^2}}, \tag{9}$$

where μ is the point forecast from each model and σ is the variance of the power output distribution. The value of variance is carefully selected by examining the training data. Specifically, historical data is divided into training and validation data. The variance is adjusted to best fit the validation data.

The variance selected for the Gaussian distribution can be constant or vary based on time of the day. This assumption is evaluated by the probability integral transform (PIT), expressed by the cumulative distribution function of the forecasts.

The PIT value is derived from the cumulative distribution function $F(\cdot)$ of the forecast (Verbois et al., 2018):

$$\text{PIT} = \begin{cases} F(P), & P \geqslant 0 \\ U(0, 1), & P = 0 \end{cases}, \tag{10}$$

where P is the measured power output and $U(0, 1)$ is a random number from a uniform distribution between 0 and 1. When plotting the PIT histogram, the best fitting probabilistic distribution to the data will have a uniform histogram.

3.3.2. Quantile regression

Quantile regression is a regression model that minimizes loss functions for specified quantiles (Liu et al., March 2017). The q^{th} quantile of response variable y can be expressed by:

$$Q_y(q|X_t) = X_t\beta_q, \tag{11}$$

where X_t are the regressed instances of the power output, and β_q is a vector of parameters for each quantile. The predicted q^{th} quantile $Q_y(q|X_t)$ can be obtained by minimizing the loss function:

$$\min_{\beta_q}\left[\sum_{\{t:y_t \geq X_t\beta_q\}} q\left|y_t - X_t\beta_q\right| + \sum_{t:y_t < X_t\beta_q}\left(1-q\right)\left|y_t - X_t\beta_q\right|\right]. \tag{12}$$

4. Posterior forecast distribution with copulas

With the prior forecast distribution of solar power, we can use temperature data to update the forecasting to posterior forecast distribution. Let p denote power and t denote temperature. According to (1), the posterior distribution for solar power given the temperature is:

$$f\left(p \middle| T = t\right) = \frac{f_{PT}(p, t)}{f_T(t)}. \tag{13}$$

In this section, we review how the conditional probability is computed using the copula-based method in (Nelsen, 2006).

4.1. Joint probability distribution and copulas

Based on Sklar's theorem the joint probability distribution between two univariate marginal distributions can be described by a copula. For

a d-dimensional joint PDF, the copula can be expressed as:

$$C(F_1(x_1),...,F_d(x_d)) = F(x_1,...,x_d) = \mathbb{P}(X_1 \leqslant x_1,...,X_d \leqslant x_d), \quad (14)$$

where $C(\cdot)$ is the copula, and $F_i(\cdot)$ is the uniform marginal probability distribution, i.e., the cumulative distribution function (CDF) for variable x_i.

Accordingly, the joint CDF between power and temperature can be described using copula:

$$F_{PT}(p, t) = C(F_P(p), F_T(t)). \quad (15)$$

Taking the derivative of this equation yields the joint PDF (Patton, 2001):

$$f_{PT}(p, t) = \frac{\partial^2}{\partial p \cdot \partial t} F(p, t) = \frac{\partial^2}{\partial p \cdot \partial t} C(F_P(p), F_T(t)) = c(F_P(p), F_T(t)) \cdot f_P(p) \cdot f_T(t), \quad (16)$$

where c is the copula density function for power and temperature.

Replacing $f_{PT}(p, t)$ in (13) using (16), one can obtain the posterior distribution of solar power:

$$F_{PT}(p, t) = C(F_P(p), F_T(t)). \quad (17)$$

The conditional probability density function (PDF) can be further expressed by:

$$f(p|T = t) = f_P(p) \cdot c(F_P(p), F_T(t)), \quad (18)$$

where $F_P(p)$ is the prior distribution obtained in Section 3. Therefore, to obtain the posterior distribution becomes to derive copulas between two marginal CDFs of solar power and temperature.

4.2. Estimating copulas

Parametric copulas or empirical copulas can be used to describe the dependencies between solar power and temperature. Parametric copulas pre-select the structure of dependencies and estimate parameters from data. In contrast, empirical copulas do not make an underlying assumption of dependency structure but directly fit the joint probability using data.

4.2.1. Parametric copulas

Three parametric copulas are adopted to capture the dependencies between solar power and temperature. In each of the parametric copulas (Namely Gaussian, T and Frank copula), the corresponding parameters are calculated based on the training set using maximum likelihood estimation. The description of copula families can be found in (Nelsen, 2006).

4.2.2. Empirical copulas

Empirical copulas do not assume a specific structure as in parametric copulas. Rather, kernel density estimation (KDE) is commonly used to estimate the empirical copulas from the data. A number of kernel functions K with bandwidth h are placed around N data points. In our paper, a multivariate KDE (two-dimensional) is formed to estimate the copula as follows:

$$\hat{c}(F_P(p), F_T(t)) = \frac{1}{N \cdot h_p \cdot h_t} \sum_{i=1}^{N} K\left(\frac{F_P(p) - R_P(P_i)}{h_p}\right) \cdot K\left(\frac{F_T(t) - R_T(T_i)}{h_t}\right). \quad (19)$$

The empirical copulas are derived using the ranking mechanism to represent the CDF. Specifically, $R_P(P_i)$ and $R_T(T_i)$ are the normalized ranks of solar power and temperature, given by:

Table 2
Example dataset and the corresponding ranking.

Point	Power	Temperature	Power rank	Temperature rank
1	9	93	0.95	1
2	7	78	0.75	0.6
3	3.6	75	0.4	0.45
4	2.5	72	0.25	0.2
5	1.8	73	0.15	0.25
6	8.5	85	0.85	0.85
7	7.3	84	0.8	0.8
8	4.1	76	0.45	0.5
9	6.5	79	0.65	0.65
10	5.9	80	0.6	0.7
11	3.4	73	0.35	0.25
12	2.7	92	0.3	0.95
13	1.4	74	0.1	0.35
14	6.8	69	0.7	0.05
15	9.5	77	1	0.55
16	0.5	71	0.05	0.15
17	5.8	70	0.55	0.1
18	8.6	89	0.9	0.9
19	4.7	74	0.5	0.35
20	2.1	81	0.2	0.75

$$R_P(p_i) = \frac{1}{N} \sum_{j=1}^{n} \mathbb{1}\{p_j \leqslant p_i\}. \quad (20)$$

$$R_T(t_i) = \frac{1}{N} \sum_{j=1}^{n} \mathbb{1}\{t_j \leqslant t_i\}. \quad (21)$$

An example is given to show how the copula is derived. Table 2 gives 20 example data points of power and temperature. The first step is to rank the data points and the ranks are given in column 4 and 5. Note that the resulted rankings are essentially CDFs between [0, 1]. In order to generate the copula, a 2-dimensional kernel is placed on each of the rankings, and then the copula is formed by adding all the kernels. The copula of the example dataset is depicted in Fig. 4. Note that the shape of the copula depends on the kernel bandwidth. The resulted copula will be used to compute posterior probability distribution of solar power given temperature data.

5. Test design and performance evaluation

5.1. Test design

Year 2015 data are used for training and Year 2016 data are used for testing. Specifically in 2016, the months of January, April, July, and October are chosen to represent four seasons. In addition, in order to

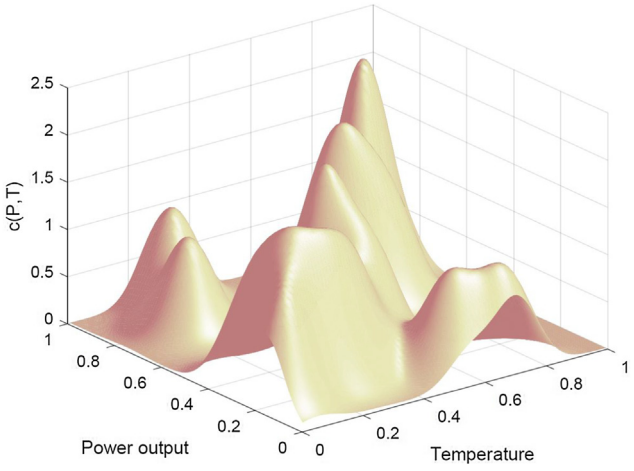

Fig. 4. Copula Density function for the example dataset.

have a comprehensive testing for the year around, one location and one point forecasting model are selected with rolling forecasting for the whole year of 2016. The performance metrics are averaged across all days and reported in Section 6.

The power data are normalized by the maximum and minimum amount from the training period, similar to Sharma et al. (2016). The negative values in power are set to zero.

5.2. Evaluation criteria

To evaluate the performance of probabilistic forecasting, the pinball loss, continues ranked probability score (CRPS), prediction interval coverage probability (PICP) and prediction interval normalized width (PINAW) are used.

5.3. Pinball loss

Pinball loss is an error measure for quantile forecasts. $\hat{y}_{t,q}$ is the forecasted point for the q^{th} quantile and time t and y_t is the actual data for that time (van der Meer et al., 2018). The Pinball loss can be written as:

$$\text{Pinball}\left(\hat{y}_{t,q}, y_t, q\right) = \begin{cases} (1-q)(\hat{y}_{t,q} - y_t), & y_t < \hat{y}_{t,q} \\ q(\hat{y}_{t,q} - y_t), & y_t \geqslant \hat{y}_{t,q} \end{cases}. \tag{22}$$

Pinball loss is calculated for each quantile separately. A lower pinball loss indicates better probabilistic forecasting performance. In the paper, a daily average of pinball loss (the sum of pinball loss averaged over the 7 day test period) is calculated and reported.

5.4. CRPS

The other method used for evaluation of the probabilistic forecasts is the continuous ranked probability score (CRPS). Given a cumulative forecast function $\hat{F}_t$ and an observation of the actual power generated y_t, the CRPS is defined as follows (Yang et al., 2018):

$$CRPS\left(\hat{F}_t, y_t\right) = \int_{-\infty}^{+\infty} \left(\hat{F}_t(\hat{y}_t) - \mathbb{1}\{\hat{y}_t \geqslant y_t\}\right)^2 d\hat{y}. \tag{23}$$

The CRPS skill score is also calculated in this study. Two benchmarks similar to the complete-history persistence ensemble (CH-PeEn) model are developed based on the data in year 2015 (Yang, 2019a).

The CRPS skill score (CSS) is calculated as described below:

$$CSS = 1 - \frac{CRPS_{Model}}{CRPS_{Benchmark}}. \tag{24}$$

5.5. PICP

Prediction interval coverage probability (PICP) is used to evaluate the coverage of the actual output by the forecast interval. The PICP for a α% prediction interval which covers from $\frac{100-\alpha}{2}$ to $\frac{100+\alpha}{2}$ percentiles is given as below:

$$PICP = \frac{1}{N}\sum_{t=1}^{N} 1\left(\hat{P}_{\frac{100-\alpha}{2}}(t) < P(t) < \hat{P}_{\frac{100+\alpha}{2}}(t)\right), \tag{25}$$

where P(i) is the actual power output at time t and $\hat{P}_i(t)$ is the i^{th} percentile of the forecast at time t.

5.6. PINAW

Prediction interval normalized width (PINAW) is the average interval width for the α% prediction interval normalized by the actual power output. This metric is used to determine the sharpness of the forecasts. PINAW for the α% interval at time t can be defined as:

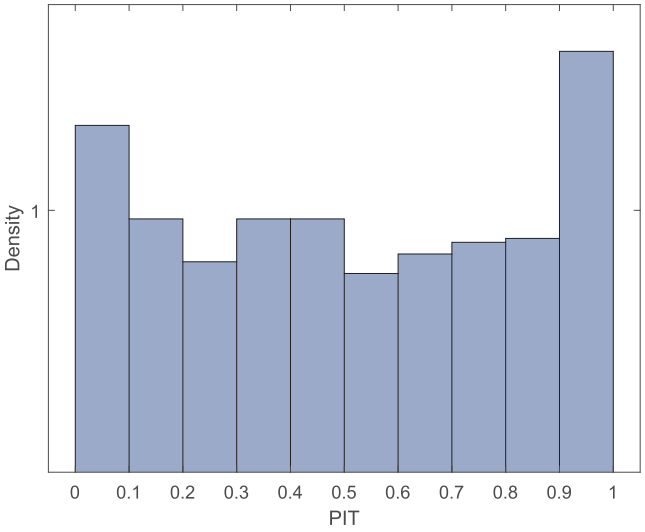

Fig. 5. PIT histogram of the prior probabilistic forecast assuming Gaussian distribution with constant variance.

$$PINAW(t) = \frac{\hat{P}_{\frac{100+\alpha}{2}}(t) - \hat{P}_{\frac{100-\alpha}{2}}(t)}{\overline{P(t)}}, \tag{26}$$

where $\overline{P(t)}$ is the average power output for the time t during the training period.

6. Results and discussions

In this section, the probabilistic forecasting results are analyzed and compared. The instructions for reproducing the results are presented in the Appendix.

6.1. Bayesian prior forecasting

Using only historical power data, we generate prior forecast distribution using two versions of Gaussian assumptions and quantile regression. First, we assume Gaussian Distribution with constant variance and plot PIT histogram as shown in Fig. 5.

Note that PIT is U-Shaped instead of having a uniform distribution, which indicate the assumption of constant variance fails to account for the changing variance of data for different time of Day (ToD). Therefore we adjust the variance based on Year 2015 data for the same ToD. The PIT histogram of the Gaussian distribution with time-varying variance is shown in Fig. 6. It is observed that the Gaussian distribution with time-varying variance fits the solar output more accurately as its shape resembles a uniform distribution.

Quantile regression is also used to generate prior probabilistic forecast. Comparing with the Gaussian assumption, the average performance metrics are reported in Table 3. It is observed that both Pinball loss and CRPS are better using the Gaussian assumption than quantile regression. Though quantile regression shows a slightly better PICP, the forecast interval is significantly wider than that with the Gaussian assumption.

6.2. Prior distribution vs. posterior distribution

Posterior distribution is obtained by multiplying the prior distribution and the temperature-power copula as described in (18). The copulas are generated using year 2015s power and temperature data. The copula captures the underlying relation between the solar power and temperature.

The prior and posterior density functions of solar power are presented in Fig. 7. The trends are the same, but some noticeable changes

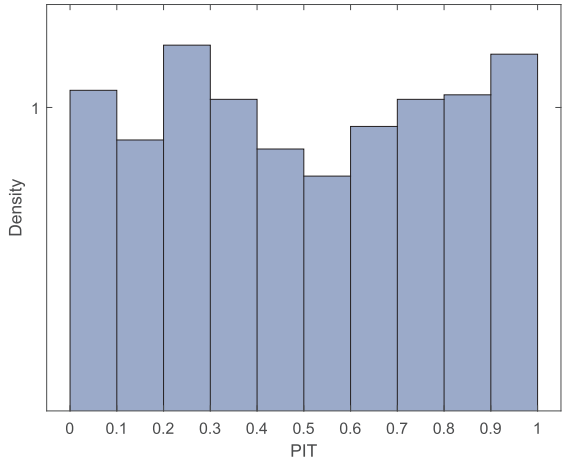

Fig. 6. PIT histogram of the probabilistic forecast assuming Gaussian distribution with changing variance.

Table 3
Comparison between Gaussian and QR probabilistic forecasts.

Forecast Method	Pinball loss	CRPS	PICP	PINAW
Gaussian	0.0249	0.0237	0.8025	0.4881
QR	0.0388	0.0284	0.8464	0.7483

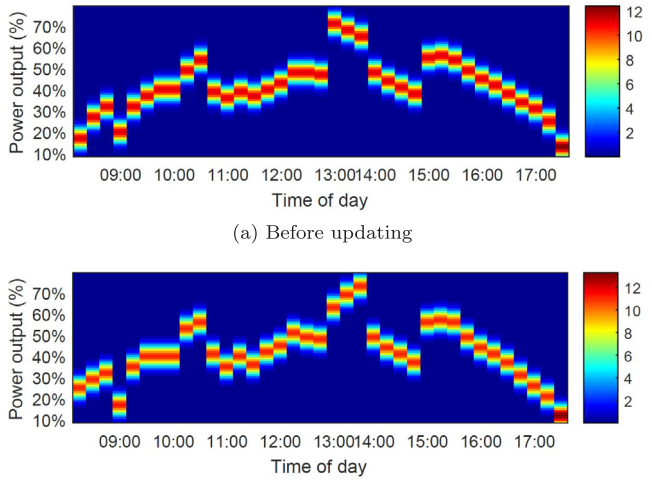

(a) Before updating

(b) After updating

Fig. 7. Heat map of the forecasts (a) before and (b) after updating for February 1st 2016 at Bayshore elementary school.

are observed, such as from 13:00 to 14:00 where the temperature is deemed strongly correlated with the power. To further quantify the prior and posterior probabilistic forecasts, the accuracy of the forecasts are evaluated using pinball loss (shown in Fig. 8). It is observed that the posterior forecasts yield lower pinball losses for all cases.

6.3. Parametric copulas vs. empirical copulas

Empirical copulas and three parametric copulas are tested. Parametric copulas pre-defines the copula structure, so that corresponding parameters can be quickly calculated. Empirical copulas fit the joint distribution using kernels on data, which might be more accurate but time consuming. We compare the results of all four types of copulas in terms of pinball loss and computational time.

Fig. 9 depicts the Gaussian copula and empirical copula for the Bayshore elementary school. One can see that empirical copula

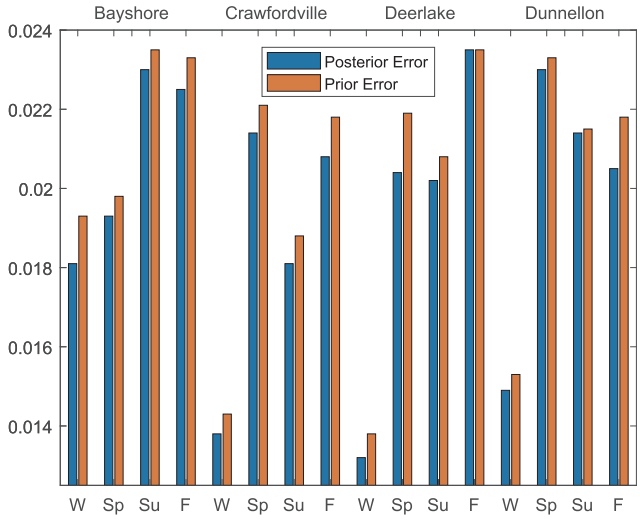

Fig. 8. The Pinball loss comparison between prior and posterior forecasts using ANN models.

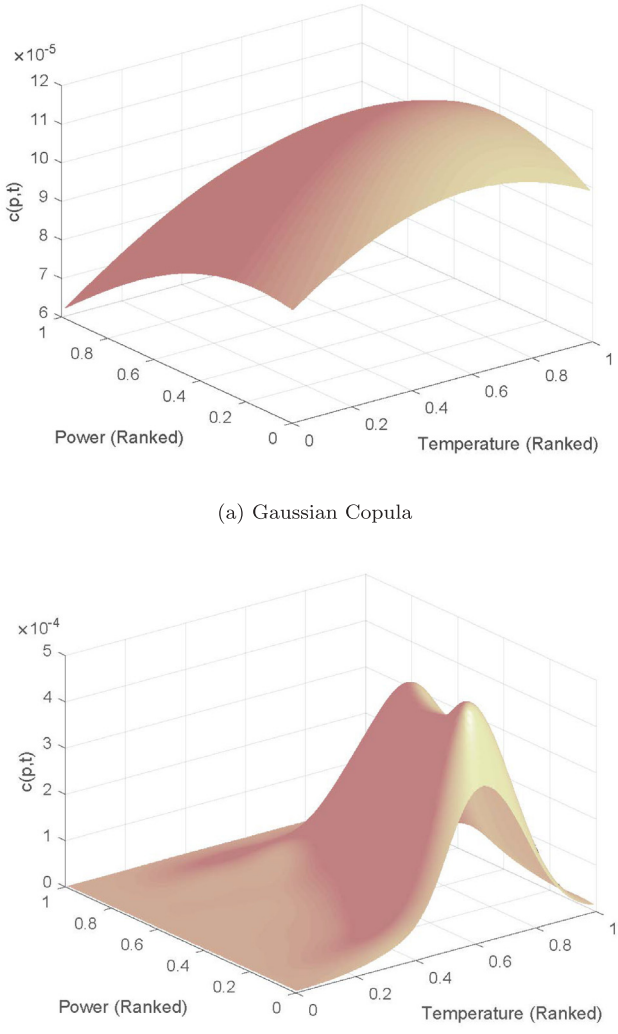

(a) Gaussian Copula

(b) Empirical Copula

Fig. 9. Two copulas for Bayshore elementary school using 2015 data.

Table 4
Average Pinball loss and run-time comparison between the copula methods.

Copula Method	Gaussian	t	Frank	Empirical
Pinball loss	0.011495	0.011411	0.011394	0.011307
Computational time(s)	0.5388	2.4942	0.1783	12.3327

provides a refined fit to the data. Table 4 shows the average pinball loss and computational time for different copulas. It is clearly seen that empirical copulas outperforms parametric copulas in the accuracy with lower pinball loss. However, the computational time is dramatically increased. Note that in our studies, all the copulas are estimated offline using previous year's data. If online forecasting needs to be implemented with copulas estimated in real time, the trade-off between accuracy and computational time should be taken into account.

6.4. Bayesian forecasting vs. benchmark models

Two persistent ensemble models are developed as benchmark to quantify the Bayesian forecasting performance. The CH-PeEn model uses all the data from 2015 to calculate the percentiles of the probability distribution. Another PeEn method with 20 members uses selected days from 2015. Both benchmark models are conditioned on time of the day. Figs. 10 and 11 show the probability distribution of power from the benchmark models at the Bayshore elementary school. Using these two models, the CRPS skill scores of Bayesian forecasting in different locations are presented in Table 5. One can see that the Bayesian forecasting has a significant improvement over the benchmark models.

6.5. Bayesian forecasting vs. TaaF forecasting

For TaaF forecasting, we use both solar power and temperature data as inputs to the five underlying models and obtain probabilistic forecasts with quantile regression and Gaussian distribution. Parameters of TaaF forecasting are optimally tuned for the training and validation data to insure that TaaF performance is on par with the state of the art. Indeed, when evaluating TaaF we found that good performance metrics are also achieved. Fig. 12 shows the probabilistic forecasting results from TaaF forecasting and the proposed Bayesian forecasting. Both methods perform very well, while the Bayesian forecasting covers some

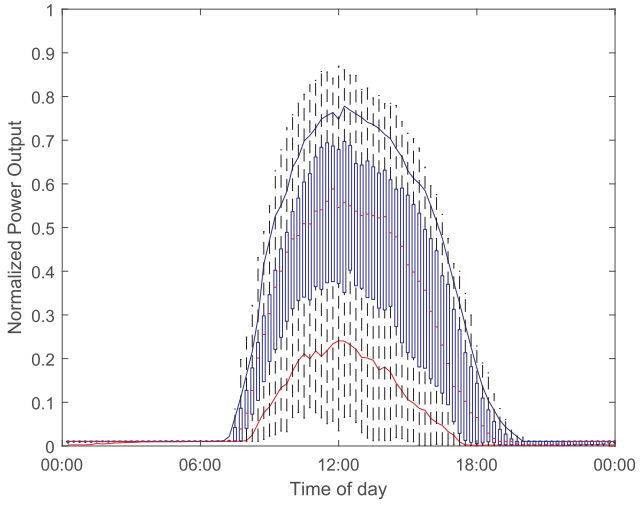

Fig. 10. The box plot (dotted red line represents the mean) alongside the 10% (red line) and 90% (blue line) Probability Distribution of power for the CH-PeEn benchmark model for Bayshore elementary school. (For interpretation of the references to colour in this figure legend, the reader is referred to the web version of this article.)

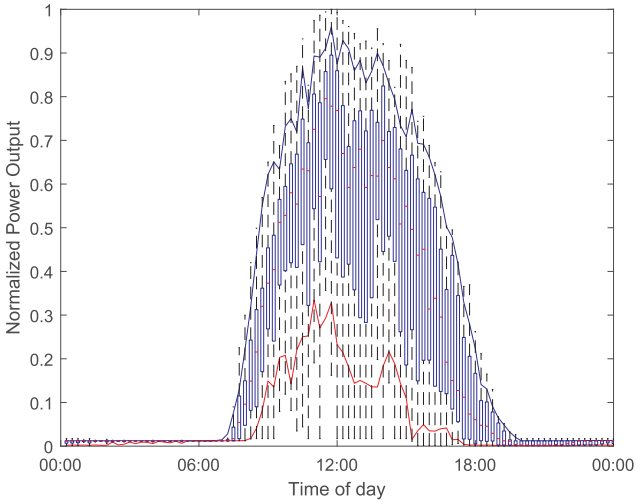

Fig. 11. The box plot (dotted red line represents the mean) alongside the 10% (red line) and 90% (blue line) Probability Distribution of power for the PeEn benchmark model with 20 members for Bayshore elementary school. (For interpretation of the references to colour in this figure legend, the reader is referred to the web version of this article.)

Table 5
The average CRPS skill for all four locations.

Location		Bayshore	Crawfordville	Deerlake	Dunnellon
Season	Benchmark				
Winter	CH-PeEn	0.48396	0.79868	0.84998	0.81524
	20 Member PeEn	0.57786	0.7895	0.81282	0.70852
Spring	CH-PeEn	0.36908	0.64324	0.63666	0.582925
	20 Member PeEn	0.45062	0.6247	0.56822	0.365575
Summer	CH-PeEn	0.28934	0.6614	0.70058	0.67472
	20 Member PeEn	0.39114	0.65174	0.63798	0.51726
Fall	CH-PeEn	0.28126	0.61746	0.58284	0.70794
	20 Member PeEn	0.38072	0.60338	0.50732	0.55944

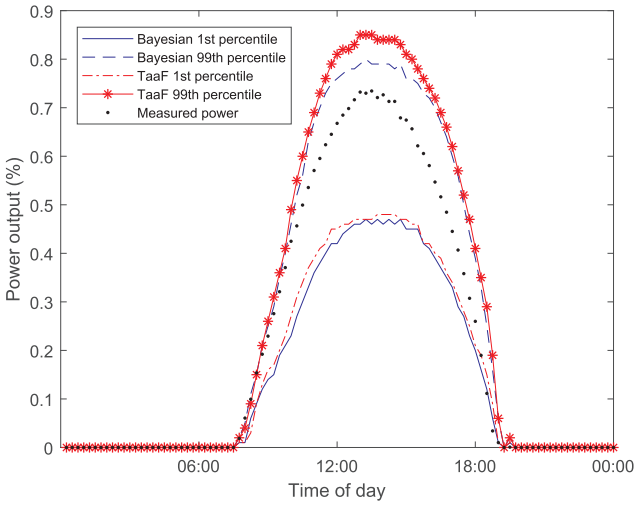

Fig. 12. TaaF and Bayesian forecasting for May 1st at Deerlake Middle School.

of the points better than the TaaF method, e.g., the points near sunrise and sunset. Also, the Bayesian forecast has a narrower interval especially in the mid-day. Below we discuss the performance in detail using representative days in four seasons and the whole year.

6.5.1. Four seasons

The forecasts are generated for all the locations and the

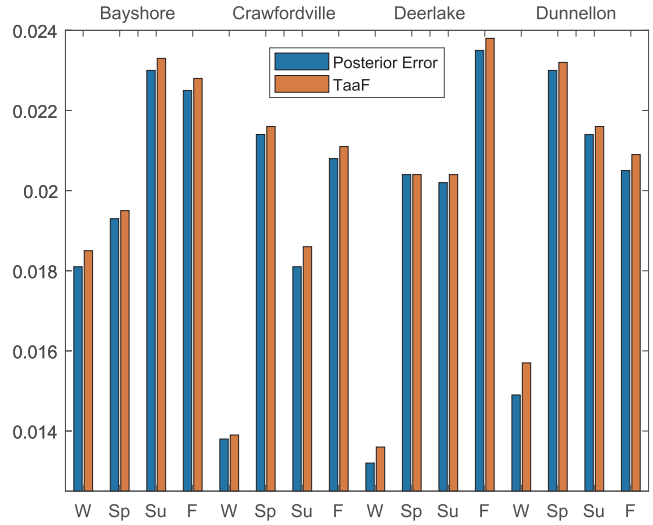

Fig. 13. The Pinball loss comparison between Bayesian and TaaF forecasting using ANN models.

representative days selected during each season. Fig. 13 shows the pinball losses of Bayesian forecasting and TaaF forecasting using the ANN model. The amount of improvement varies in different seasons, but Bayesian forecasting in most cases outperforms TaaF forecasting. TaaF show better results in three cases of Winter and Spring at Crawfordville and the Summer case at Dunnellon high school, but it is outperformed by Bayesian forecasting for the rest 13 cases.

The average improvement of pinball loss for the proposed method compared to the TaaF method is 4.19%. To examine if this improvement is restricted to a specific point forecasting model, the pinball losses for all five underlying models are calculated and presented in Table 6. In 73 out of 80 test cases, the results of the posterior are better than the TaaF forecast.

Specifically, the overall average improvements using ANN, GB, MLR, RF, and ARIMA models are 2.09%, 2.77%, 5.54%, 3.24%, and 8.33% respectively.

The CRPS of the Bayesian and TaaF model are also calculated for all the test cases and presented in Table 7. The CRPS improvement for the ANN, GB, MLR, RF, and ARIMA models when using the empirical copula to update the forecasts are 2.06%, 2.86%, 8.15%, 3.42%, and 13.55% over the TaaF model. The CRPS of the Bayesian method is showing improvement over the TaaF method when averaged across all methods, seasons and locations. Overall the CRPS is 5.65% better in the case of the Bayesian method compared to TaaF.

The average PICP and PINAW across all locations and seasons for different forecasting models are also reported in Table 8. The results indicate the Bayesian method in general has a better coverage with narrower intervals.

Table 6
The average pinball loss for all five models.

Model		ANN	GB	MLR	RF	ARIMA
Season	Method					
Winter	TaaF	0.021575	0.022175	0.0216	0.021975	0.019125
	Bayesian	0.02125	0.02165	0.021575	0.02185	0.0188
Spring	TaaF	0.027725	0.027975	0.027725	0.0279	0.03125
	Bayesian	0.027025	0.027075	0.0273	0.027325	0.02775
Summer	TaaF	0.026075	0.026025	0.029825	0.0277	0.027325
	Bayesian	0.025625	0.02545	0.02575	0.026075	0.026275
Fall	TaaF	0.027675	0.02765	0.028425	0.02835	0.029275
	Bayesian	0.026575	0.02685	0.0273	0.02735	0.025925

Table 7
The average CRPS for all four locations.

Location		Bayshore	Crawfordville	Deerlake	Dunnellon
Season	Method				
Winter	TaaF	0.02624	0.01724	0.01418	0.01692
	Bayesian	0.02558	0.01664	0.01396	0.01684
Spring	TaaF	0.02942	0.02754	0.02638	0.031748
	Bayesian	0.02638	0.0253	0.02574	0.03038
Summer	TaaF	0.0344	0.02442	0.02898	0.03158
	Bayesian	0.03066	0.02432	0.02626	0.02876
Fall	TaaF	0.03104	0.02638	0.03122	0.02724
	Bayesian	0.0296	0.02408	0.03048	0.02592

Table 8
The average PICP and PINAW across all data reported for each forecast model.

Model		ANN	GB	MLR	RF	ARIMA
Criteria	Method					
PICP	TaaF	0.814838	0.812238	0.750017	0.813975	0.788144
	Bayesian	0.813988	0.810088	0.795047	0.815113	0.798175
PINAW	TaaF	0.424169	0.425213	0.428487	0.424756	0.438038
	Bayesian	0.414519	0.414213	0.414833	0.41425	0.424119

Table 9
Comparison between Bayesian and TaaF probabilistic forecasts during 2016 at Bayshore elementary.

Forecast Method	Pinball loss	CRPS	PICP	PINAW
Bayesian	0.0249	0.0237	0.8025	0.4881
TaaF	0.0253	0.0242	0.8023	0.4928

6.5.2. *Year 2016 rolling testing*

Additionally, we select one location (Bayshore) and one model (MLR) to conduct a rolling 7-day testing for the whole year of 2016. The performance metrics are averaged across all days and reported in Table 9.

The results show that the application of copula-based Bayesian forecasting to the short-term solar forecasting problem is successful. Overall the Bayesian forecasting has higher accuracy, better coverage, and narrower intervals.

7. Conclusion

Achieving higher accuracy in solar generation forecasting can help operators to devise a better operation plan for the power system. This study applies Bayesian forecasting using copulas to improve prior probabilistic forecasting. Results show that copulas effectively capture the joint probability distribution of solar power and temperature. The FSEC database is used and numerical results show that Bayesian forecasting with conditional PDFs derived from power-temperature copulas outperforms TaaF forecasting that uses temperature as a feature. Future work will explore higher-dimensional copulas that incorporate more exogenous features and use spatio-temporal models to increase the accuracy of forecasts.

Appendix A. Supplementary material

The data and code can be found on GitHub for reproducibility Panamtash, 2018. The code for point forecasting is written in R and Python. The code for copula-based Bayesian probabilistic forecasting is written in MATLAB.

Packages used in R are ‘forecast’,‘tseries’, ‘quantreq’, ‘neuralnet’, and ‘gbm’. The python version is 2.7 and the packages used are

'numpy', 'csv', 'math', 'array', and 'sklearn'.

Data: The data folder contains power and temperature data for all locations from the FSEC database from 2015 to 2017. It also contains the point forecasting results for all locations and seasons using the five different models with and without temperature as an input. The intermediate results of copulas are also included in the data folder.

Code: The code folder contains code for point forecasting models, code for parametric and empirical copulas, code for Bayesian forecasting models, and code for the benchmark model. All the results presented in this document can be reproduced with the file named *final*. The code needs to be executed for all locations, seasons and models. The only change necessary in the code is to add the directory of files.

Appendix B. Supplementary material

Supplementary data associated with this article can be found, in the online version, at https://doi.org/10.1016/j.solener.2019.11.079.

References

Innovation education. <http://www.energywhiz.com/>.

André, M., Perez, R., Soubdhan, T., Schlemmer, J., Calif, R., Monjoly, S., 2019. Preliminary assessment of two spatio-temporal forecasting technics for hourly satellite-derived irradiance in a complex meteorological context. Sol. Energy 177, 703–712. https://doi.org/10.1016/j.solener.2018.11.010. ISSN 0038-092X. http://www.sciencedirect.com/science/article/pii/S0038092X18311101.

Bessa, R.J., Miranda, V., Botterud, A., Zhou, Z., Wang, J., 2012. Time-adaptive quantile-copula for wind power probabilistic forecasting. Renew. Energy 40 (1), 29–39. https://doi.org/10.1016/j.renene.2011.08.015. ISSN 0960-1481.

Bright, J.M., Babacan, O., Kleissl, J., Taylor, P.G., Crook, R., 2017. A synthetic, spatially decorrelating solar irradiance generator and application to a lv grid model with high pv penetration. Sol. Energy 147, 83–98. https://doi.org/10.1016/j.solener.2017.03.018. ISSN 0038-092X. http://www.sciencedirect.com/science/article/pii/S0038092X17301780.

Davis, K.O., Kurtz, S.R., Jordan, D.C., Wohlgemuth, J.H., Sorloaica-Hickman, N., 2013. Multi-pronged analysis of degradation rates of photovoltaic modules and arrays deployed in Florida. Prog. Photovolt. Res. Appl. 21 (4), 702–712. https://doi.org/10.1002/pip.2154.

Engerer, N., Mills, F., 2014. Kpv: a clear-sky index for photovoltaics. Sol. Energy 105, 679–693. https://doi.org/10.1016/j.solener.2014.04.019. ISSN 0038-092X. http://www.sciencedirect.com/science/article/pii/S0038092X14002151.

Fliess, M., Join, C., Voyant, C., 2018. Prediction bands for solar energy: new short-term time series forecasting techniques. Sol. Energy 166, 519–528. https://doi.org/10.1016/j.solener.2018.03.049. ISSN 0038-092X. http://www.sciencedirect.com/science/article/pii/S0038092X18302810.

Hemmati, R., Saboori, H., 2017. Stochastic optimal battery storage sizing and scheduling in home energy management systems equipped with solar photovoltaic panels. Energy Build. 152, 290–300. https://doi.org/10.1016/j.enbuild.2017.07.043. ISSN 0378-7788. http://www.sciencedirect.com/science/article/pii/S0378778817300373.

Hong, T., Xie, J., Black, J., 2019. Global energy forecasting competition 2017: hierarchical probabilistic load forecasting. Int. J. Forecast. 35 (4), 1389–1399. https://doi.org/10.1016/j.ijforecast.2019.02.006. ISSN 0169-2070. http://www.sciencedirect.com/science/article/pii/S016920701930024X.

Killinger, S., Engerer, N., Müller, B., 2017. Qcpv: a quality control algorithm for distributed photovoltaic array power output. Sol. Energy 143, 120–131. https://doi.org/10.1016/j.solener.2016.12.053. ISSN 0038-092X. http://www.sciencedirect.com/science/article/pii/S0038092X16306600.

Koopman, S.J., Lit, R., Lucas, A., Opschoor, A., 2018. Dynamic discrete copula models for high-frequency stock price changes. J. Appl. Economet. 33 (7), 966–985. https://doi.org/10.1002/jae.2645. https://onlinelibrary.wiley.com/doi/abs/10.1002/jae.2645.

Liu, B., Nowotarski, J., Hong, T., Weron, R., 2017. Probabilistic load forecasting via quantile regression averaging on sister forecasts. IEEE Trans. Smart Grid 8 (2), 730–737. https://doi.org/10.1109/TSG.2015.2437877. ISSN 1949-3053.

Lynn, K., Szaro, J., Wilson, W., Healey, M., 2006. A review of pv system performance and life-cycle costs for the sunsmart schools program. Sol. Energy. https://doi.org/10.1115/isec2006-99112.

C. Marcy. U.s. energy information administration - eia - independent statistics and analysis, Mar 2019. <https://www.eia.gov/todayinenergy/detail.php?id=38752>.

Munkhammar, J., Widén, J., Hinkelman, L.M., 2017. A copula method for simulating correlated instantaneous solar irradiance in spatial networks. Sol. Energy 143, 10–21. https://doi.org/10.1016/j.solener.2016.12.022. ISSN 0038-092X. http://www.sciencedirect.com/science/article/pii/S0038092X16306168.

Munkhammar, J., van der Meer, D., Widén, J., 2019. Probabilistic forecasting of high-resolution clear-sky index time-series using a markov-chain mixture distribution model. Sol. Energy 184, 688–695. https://doi.org/10.1016/j.solener.2019.04.014. ISSN 0038-092X. http://www.sciencedirect.com/science/article/pii/S0038092X19303469.

Murata, A., Ohtake, H., Oozeki, T., 2018. Modeling of uncertainty of solar irradiance forecasts on numerical weather predictions with the estimation of multiple confidence intervals. Renew. Energy 117, 193–201. https://doi.org/10.1016/j.renene.2017.10.043. ISSN 0960-1481. http://www.sciencedirect.com/science/article/pii/S0960148117309813.

Nelsen, R.B., 2006. 2 ed. An Introduction to Copulas, vol. 4 Springer ISBN 978-0-387-28678-5.

Panamtash, H., 2018. Code implementation, December 2018. <https://github.com/hpanamtash/Bayesian_Forecasting>.

Panamtash, H., Zhou, Q., 2018. Coherent probabilistic solar power forecasting. 2018 International Conference on Probabilistic Methods Applied to Power Systems (PMAPS), (5):1–6, 2018.

Patton, A.J., 2001. Modelling time-varying exchange rate dependence using the conditional copula. SSRN Electron. J. https://doi.org/10.2139/ssrn.275591.

Pawar, P., Cortés, C., Murray, K., Kleissl, J., 2019. Detecting clear sky images. Sol. Energy 183, 50–56. https://doi.org/10.1016/j.solener.2019.02.069. ISSN 0038-092X. http://www.sciencedirect.com/science/article/pii/S0038092X19302130.

Pedro, H.T., Coimbra, C.F., David, M., Lauret, P., 2018. Assessment of machine learning techniques for deterministic and probabilistic intra-hour solar forecasts. Renew. Energy 123, 191–203. https://doi.org/10.1016/j.renene.2018.02.006. ISSN 0960-1481. http://www.sciencedirect.com/science/article/pii/S0960148118301423.

Saint-Drenan, Y., Good, G., Braun, M., 2017. A probabilistic approach to the estimation of regional photovoltaic power production. Sol. Energy 147, 257–276. https://doi.org/10.1016/j.solener.2017.03.007. ISSN 0038-092X. http://www.sciencedirect.com/science/article/pii/S0038092X17301676.

Sharma, V., Yang, D., Walsh, W., Reindl, T., 2016. Short term solar irradiance forecasting using a mixed wavelet neural network. Renew. Energy 90, 481–492. https://doi.org/10.1016/j.renene.2016.01.020. ISSN 0960-1481. http://www.sciencedirect.com/science/article/pii/S0960148116300209.

Shepero, M., van der Meer, D., Munkhammar, J., Widén, J., 2018. Residential probabilistic load forecasting: a method using gaussian process designed for electric load data. Appl. Energy 218, 159–172. https://doi.org/10.1016/j.apenergy.2018.02.165. ISSN 0306-2619. http://www.sciencedirect.com/science/article/pii/S030626191830299X.

van der Meer, D., Munkhammar, J., Widén, J., 2018. Probabilistic forecasting of solar power, electricity consumption and net load: Investigating the effect of seasons, aggregation and penetration on prediction intervals. Sol. Energy 171, 397–413. https://doi.org/10.1016/j.solener.2018.06.103. ISSN 0038-092X. http://www.sciencedirect.com/science/article/pii/S0038092X18306522.

van der Meer, D., Widén, J., Munkhammar, J., 2018. Review on probabilistic forecasting of photovoltaic power production and electricity consumption. Renew. Sustain. Energy Rev. 81, 1484–1512. https://doi.org/10.1016/j.rser.2017.05.212. ISSN 1364-0321. http://www.sciencedirect.com/science/article/pii/S1364032117308523.

Verbois, H., Huva, R., Rusydi, A., Walsh, W., 2018. Solar irradiance forecasting in the tropics using numerical weather prediction and statistical learning. Sol. Energy 162, 265–277. https://doi.org/10.1016/j.solener.2018.01.007. ISSN 0038-092X. http://www.sciencedirect.com/science/article/pii/S0038092X18300197.

Verbois, H., Rusydi, A., Thiery, A., 2018. Probabilistic forecasting of day-ahead solar irradiance using quantile gradient boosting. Sol. Energy 173, 313–327. https://doi.org/10.1016/j.solener.2018.07.071. ISSN 0038-092X. http://www.sciencedirect.com/science/article/pii/S0038092X18307357.

Widén, J., Shepero, M., Munkhammar, J., 2017. On the properties of aggregate clear-sky index distributions and an improved model for spatially correlated instantaneous solar irradiance. Sol. Energy 157, 566–580. https://doi.org/10.1016/j.solener.2017.08.033. ISSN 0038-092X. http://www.sciencedirect.com/science/article/pii/S0038092X17307132.

Yang, D., 2019a. A universal benchmarking method for probabilistic solar irradiance forecasting. Sol. Energy 184, 410–416. https://doi.org/10.1016/j.solener.2019.04.018. ISSN 0038-092X. http://www.sciencedirect.com/science/article/pii/S0038092X19303457.

Yang, D., 2019b. Post-processing of nwp forecasts using ground or satellite-derived data through kernel conditional density estimation. J. Renew. Sustain. Energy 11 (2), 026101. https://doi.org/10.1063/1.5088721.

Yang, D., Quan, H., Disfani, V.R., Liu, L., 2017. Reconciling solar forecasts: geographical hierarchy. Sol. Energy 146, 276–286. https://doi.org/10.1016/j.solener.2017.02.010. ISSN 0038-092X. http://www.sciencedirect.com/science/article/pii/S0038092X17301020.

Yang, D., Kleissl, J., Gueymard, C.A., Pedro, H.T., Coimbra, C.F., 2018. History and trends in solar irradiance and pv power forecasting: a preliminary assessment and review using text mining. Sol. Energy 168, 60–101. https://doi.org/10.1016/j.solener.2017.11.023. Advances in Solar Resource Assessment and Forecasting. ISSN 0038-092X.. http://www.sciencedirect.com/science/article/pii/S0038092X17310022.

Zheng, Y., Zhao, J., Song, Y., Luo, F., Meng, K., Qiu, J., Hill, D.J., 2018. Optimal operation of battery energy storage system considering distribution system uncertainty. IEEE Trans. Sustain. Energy 9 (3), 1051–1060. https://doi.org/10.1109/TSTE.2017.2762364.